COMPLEX THERMAL HISTORIES OF CAI-LIKE OBJECTS IN AMOEBOID OLIVINE AGGREGATES FROM THE ALHA 77307 CO3.0 CHONDRITE: CONSTRAINTS FROM MICROSTRUCTURAL STUDIES BY TEM. Jangmi Han[1] and Adrian J. Brearley[1], [1]Department of Earth and Planetary Sciences, MSC03-2040, 1University of New Mexico, Albuquerque, NM 87131, USA (E-mail: jmhan@unm.edu; brearley@unm.edu).

Introduction: Amoeboid olivine aggregates (AOAs) are the most common type of refractory inclusions in carbonaceous chondrites and are typically irregularly-shaped and fine-grained. They contain mostly forsteritic olivine and lesser, variable amounts of refractory Ca-Al-rich phases such as Al,Ti-bearing pyroxene, ±anorthite, and ±spinel. Rarely, melilite and perovskite are present. Fe,Ni-metal grains also occur commonly in AOAs. Amoeboid olivine aggregates are interpreted as the products of nebular gas-solid condensation from the cooling solar nebula, which subsequently experienced high-temperature annealing and a small degree of melting [e.g., 1,2]. In addition, refractory Ca-Al-rich phases from AOAs show clear evidence of reactions between minerals and gas [3]. Here we report microstructural observations obtained by TEM on refractory Ca-Al-rich phases in AOAs from the primitive CO3.0 chondrite, ALHA 77307 [e.g., 4] in an effort to constrain the origins and thermal histories of AOAs.

Methods: Individual AOAs from two thin sections were studied using SEM/BSE imaging and elemental X-ray mapping and then selected AOAs were sectioned using FIB techniques. Six FIB sections were prepared from refractory CAI-like objects within two AOAs (#02 and #03) and were examined in detail by TEM techniques to characterize their microstructure and microchemistry.

Results: SEM observations of two AOAs investigated in this study show that they contain ~35 vol.% CAI-like objects enclosed by forsteritic olivine grains. These objects consist predominantly of spinel and Al,Ti-bearing diopside. Melilite is found in both AOAs, whereas perovskite is found only in AOA #03. Additionally, the CAI-like objects are texturally very different.

AOA #02 contains four distinct, subrounded spinel-rich nodules. The nodules are 50-100μm in size and consist of a zoned sequence with a spinel-rich core, a layer of intergrown spinel and Al,Ti-bearing diopside, and a diopside rim. The grain boundaries between spinel core and diopside rim are highly irregular and embayed suggesting a reaction relationship between them. Melilite only occurs in the largest, 100μm-sized CAI-like object and is surrounded by spinel and diopside. In AOA #03, the CAI-like objects occur as numerous, small patches consisting of a spinel-rich core rimmed by a thin, continuous layer of Al,Ti-bearing diopside. They are irregular in shape and are dispersed throughout the whole AOA. Unlike AOA #02, minor perovskite grains, <3μm in size, occur along the grain boundaries between spinel and diopside and are not in contact with surrounding olivine grains.

Microtextures. The FIB sections from refractory objects in both AOAs consist mainly of spinel and Al,Ti-bearing diopside. The sections from the core region of refractory objects are highly compact with no evidence of pores. The spinel in the spinel-rich cores consists of an aggregate of submicron to micron-sized grains with equilibrated grain boundary microstructures, i.e., 120˚ triple junctions. However, curved and embayed interfaces between spinel and Al,Ti-bearing diopside are commonly observed, suggesting a reaction relationship between the two phases. Most grains are free of dislocations or defects, but some rare diopside and spinel grains have low densities of dislocations in localized regions.

In AOA #02, the diopside rim of the CAI-like object consists of a submicron, complex intergrowth of Al,Ti-bearing diopside, spinel, anorthite, and olivine with a highly unequilibrated grain boundary microstructures. Melilite grains from AOA #02 are highly irregular in shape and embayed by spinel and Al,Ti-rich diopside. Perovskite grains from AOA #03 are completely rimmed by a thin (0.1-0.5 μm) layer of fine-grained Al,Ti-rich diopside and spinel and are separated from melilite grains (Fig. 1). Both melilite and perovskite grains from the two AOAs indicate reaction relationships between the refractory phases and the nebular gas.

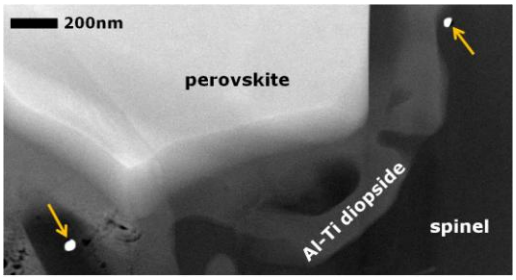

Figure 1. Dark-field STEM image of perovskite and its periphery, showing that perovskite grain is corroded by fine-grained Al,Ti-rich diopside and spinel. The arrowed grains are refractory metal-rich nanoparticles.

In one FIB section from the core region of a refractory object in AOA #02, numerous TiO_2 nanoparticles, <100nm in size, occur along some grain boundaries between spinel and pyroxene grains. The nanoparticles are crystallographically oriented with respect to spinel and are a disordered intergrowth of rutile and anatase [7].

Chemical Compositions. From the CAI-like objects in both AOAs, olivine is very close to pure forsterite and plagioclase is nearly pure anorthite. Spinel is near end-member $MgAl_2O_4$, whereas melilite is highly gehlenitic, but compositionally homogeneous. Perovskite in AOA #03 is nearly pure $CaTiO_3$. In contrast, pyroxene from both AOAs exhibits large variations in Al_2O_3 and TiO_2 contents. Generally, pyroxene in the core of the CAI-like objects contains higher Al_2O_3 and TiO_2 contents compared to pyroxene in the rims of the objects [5]. The total range of Al_2O_3 contents in pyroxene from both AOAs is 0 to 32 wt.%, and TiO_2 contents from 0 to 17 wt.%. Pyroxene grains with ≤ 10 wt.% Al_2O_3 show relatively constant TiO_2 contents ≤ 2 wt.%. The Al_2O_3 contents in pyroxene from AOA #02 progressively increase from the rim of the object towards the spinel-rich core, but the TiO_2 contents increase steeply by ~15 wt.% over a very short distance (≤ 2μm) towards the contact with the spinel-rich core. In AOA #03, pyroxene grains in contact with perovskite have the highest TiO_2 contents (16 wt.%), while those furthest away from perovskite contain <5 wt.% TiO_2.

Refractory Metal-rich Nanoparticles. Submicron refractory metal-rich nanoparticles are embedded within perovskite, spinel, melilite, and pyroxene, implying that they formed before or during condensation of all these phases. They are mostly ≤50nm in size with the largest being ~250nm. The nanoparticles within melilite or pyroxene have higher Fe concentrations than those within perovskite or spinel. All particles contain elevated, but variable concentrations of highly refractory siderophile elements such as Mo, Ru, Os, and Ir. Similar nanoparticles have been found previously in various CAIs and are widely accepted as condensation products [6].

Discussion: The microtextures and chemical compositions of refractory CAI-like objects in two AOAs indicate a high degree of textural and compositional disequilibrium implying complex thermal histories for the objects. The following observations provide clear evidence of reaction relationships between minerals and gas; i) embayed interfaces between mineral grains, particularly diopside and spinel and perovskite and spinel, ii) a complex intergrowth of fine-grained phases such as spinel, Al,Ti-bearing diopside, anorthite, and olivine in the rim of a CAI-like object in AOA #02, iii) a thin layer consisting of fine-grained spinel and Al,Ti-rich diopside surrounding perovskite grains from AOA #03, and iv) extreme compositional variations in Al,Ti-bearing diopside over very short distances. These disequilibrium textures and chemical compositions suggest that gas-solid reactions occurred under highly dynamic conditions.

Several gas-solid reactions have been proposed to explain the observed phase assemblages and chemical compositions of refractory Ca-Al-rich phases in AOAs [1,3,7,8]. Our new observations provide additional constraints on the possible processes that affected these CAI-like objects in AOAs. In refractory objects from AOA #02, we observe the replacement of melilite grains by fine-grained spinel and Al,Ti-rich diopside possibly due to a reaction between melilite, spinel, and the nebular gas. The absence of perovskite as a source of Ti in this object requires an external source of Ti to form Al,Ti-rich diopside. The textures imply a back-reaction of the nebular gas with the early condensate phases, spinel and melilite. As the reaction proceeded, TiO_2 contents in pyroxene appear to rapidly decrease outward from the interface with spinel, as Ti from the gas was incorporated into the solid phases. The disequilibrium back-reaction of spinel with Ti-saturated gas probably caused very rapid nucleation of metastable TiO_2 nanoparticles onto the surface of spinel grains. Kinetically-controlled condensation processes under disequilibrium conditions would form a simple oxide phase rather either perovskite or Ti-bearing pyroxene. Some relict melilite has survived, but most of melilite grains appear to have been consumed by the reaction. Another possible reaction between spinel and diopside to form anorthite [1] appears to be kinetically inhibited because only small amounts of anorthite are found in the rim of a CAI-like object from AOA #02. In AOA #03, perovskite has evidently undergone partial reaction to form narrow rims of fine-grained spinel and very Ti-rich Al-bearing diopside, followed by melilite. It is possible that melilite condensation is only stable once perovskite has been isolated from the nebular gas by the rim of spinel and diopside.

Conclusions: These texturally different refractory CAI-like objects in two AOAs both preserve a record of gas-solid condensation reactions under disequilibrium conditions, probably as a result of fast cooling. One possible scenario to explain these observations is that the refractory objects were transported or injected into a hotter region of the solar nebula that had undergone only partial condensation. Evidence for such transport of refractory materials is also indicated by recent isotopic studies of CAIs in the Allende [9]. Such events may be more widespread than has been previously recognized.

Acknowledgements: This work was funded by NASA grant NNG06GG37G to A. J. Brearley (PI).

References: [1] Krot A. N. et al. (2004) *Chemie der Erde, 64,* 185-239. [2] Komatsu M. et al. (2001) *Meteoritics & Planet. Sci., 36,* 629-641. [3] Han J. and Brearley A. J. (2011) *LPS XXXXII,* Abstract #1673. [4] Grossman J. N. and Brearley A. J. (2005) *Meteoritics & Planet. Sci., 40,* 87-122. [5] Hashimoto A. and Grossman L. (1987) *GCA, 51,* 1685-1704. [6] Eisenhour D. D. and Buseck P. R. (1992) *Meteoritics, 27,* 217-218. [7] Han J. and Brearley A. J. (2011) *74th Annual Meteoritical Society Meeting,* Abstract #5190. [8] Han J. and Brearley A. J. (2011) *74th Annual Meteoritical Society Meeting,* Abstract #5388. [9] Simon J. I. et al. (2011) *Science, 331,* 1175-1178.